DRAFT VERSION SEPTEMBER 13, 2012
Preprint typeset using LaTeX style emulateapj v. 12/16/11

THE RISE AND FALL OF STAR FORMATION HISTORIES OF BLUE GALAXIES AT REDSHIFTS $0.2 < z < 1.4$

CAMILLA PACIFICI,[1,2] SUSAN A. KASSIN,[3,4] BENJAMIN WEINER,[5] STÉPHANE CHARLOT,[1] JONATHAN P. GARDNER,[3] ET AL.

Draft version September 13, 2012

ABSTRACT

Popular cosmological scenarios predict that galaxies form hierarchically from the merger of many progenitors, each with their own unique star formation history (SFH). We use the approach recently developed by Pacifici et al. (2012) to constrain the SFHs of 4517 blue (presumably star-forming) galaxies with spectroscopic redshifts in the range $0.2 < z < 1.4$ from the All-Wavelength Extended Groth Strip International Survey (AEGIS). This consists in the Bayesian analysis of the observed galaxy spectral energy distributions with a comprehensive library of synthetic spectra assembled using state-of-the-art models of star formation and chemical enrichment histories, stellar population synthesis, nebular emission and attenuation by dust. We constrain the SFH of each galaxy in our sample by comparing the observed fluxes in the *B*, *R*, *I* and K_s bands and rest-frame optical emission-line luminosities with those of one million model spectral energy distributions. We explore the dependence of the resulting SFH on galaxy stellar mass and redshift. We find that the average SFHs of high-mass galaxies rise and fall in a roughly symmetric *bell-shaped* manner, while those of low-mass galaxies rise progressively in time, consistent with the typically stronger activity of star formation in low-mass compared to high-mass galaxies. For galaxies of all masses, the star formation activity rises more rapidly at high than at low redshift. These findings imply that the standard approximation of exponentially declining SFHs widely used to interpret observed galaxy spectral energy distributions is not appropriate to constrain the physical parameters of star-forming galaxies at intermediate redshifts.

Subject headings: galaxies: evolution - galaxies: star formation - galaxies: stellar content

1. INTRODUCTION

Constraints on the stellar content of galaxies are often derived from multiwavelength observations by assuming that the star formation history (SFH) of an individual galaxy can be approximated by a simple declining exponential function of the form $e^{-t/\tau}$, where t is the galaxy age and τ the star formation timescale. Such "τ-models" have been used successfully to estimate, for example, the stellar masses of nearby spiral galaxies from fits of rest-frame optical/near-infrared colors (e.g., Bell & de Jong 2001). Despite this success, an increasing number of analyses have pointed out the limitations of this approach, particularly for applications to studies of high-redshift galaxies. This is the case of Lyman-break galaxies at redshifts $z > 2$ (Papovich et al. 2001) and blue star-forming galaxies at $z \sim 2$ (Shapley et al. 2005), for which the addition of another stellar component on top of a τ-model can change the derived stellar masses by a factor of several. In fact, the major episodes of star formation in ultraviolet (UV)-luminous Lyman-break galaxies could last only a few hundred million years (Stark et al. 2009). Reddy et al. 2012 also find that, for galaxies at $1.5 < z < 4$, fits of broadband spectral energy distributions (SEDs) using exponentially declining SFHs produce star formation rates (SFRs) 5 to 10 times lower than inferred from more direct estimates based on the combined analysis of the UV and mid-infrared emission. They conclude that SFHs in which the SFR rises in time are more appropriate than declining τ-models for these galaxies. This is reinforced by the conclusion by Maraston et al. 2010 and Pforr et al. 2012 that SED fits of galaxies at $z \sim 2$ using declining τ-models produce unrealistically low ages, and that exponentially *rising* τ-models should be preferred for these galaxies. In fact, simulations of galaxy formation in a hierarchical universe predict complex SFHs, which are not well approximated by simple declining exponential laws (e.g., Lee et al. 2009; Wuyts et al. 2009).

To better characterize the SFHs of galaxies at moderate and high redshift, we require more sophisticated, physically motivated spectral analysis tools. In this Letter, we achieve this goal by appealing to the approach recently proposed by Pacifici et al. 2012 to constrain the SFHs of 4517 galaxies with secure spectroscopic redshifts in the range $0.2 < z < 1.4$. Specifically, we fit the observed broadband SEDs and emission-line strengths of these galaxies using a comprehensive library of synthetic spectra assembled by combing state-of-the-art models of stellar population synthesis, nebular emission and attenuation by dust with star formation and chemical enrichment histories derived from the semi-analytic post-treatment of a large-scale cosmological simulation. This approach allows us to characterize the SFHs of galaxies in different mass and redshift ranges in a statistically reliable manner.

The paper is organized as follows. In §2, we present observations of the *B*, *R*, *I* and K_s fluxes and rest-frame optical emission-line luminosities of 4517 blue galaxies from the All-Wavelength Extended Groth Strip International Survey (AEGIS, Davis et al. 2007). In §3, we describe the library of synthetic SEDs built to interpret these observations. We report our results in §4 and present our conclusions in §5. Throughout this Letter, we adopt a standard ΛCDM cosmology with $\Omega_M = 0.3$, $\Omega_\Lambda = 0.7$, $h = 0.7$, and a Chabrier initial mass function (Chabrier 2003).

[1] CNRS, UMR7095, Institut d'Astrophysique de Paris, F-75014, Paris, France
[2] Max Planck Institute for Astronomy, Königstuhl 17, D-69117 Heidelberg, Germany
[3] Astrophysics Science Division, Goddard Space Flight Center, Code 665, Greenbelt, MD 20771
[4] NASA Postdoctoral Program Fellow
[5] Steward Observatory, 933 North Cherry Street, University of Arizona, Tucson, AZ 85721

2. DATA

We require our observational sample to cover a large range in galaxy stellar mass and SFR. In addition, to derive good constraints on galaxy SFHs and stellar masses, we need solid spectroscopic redshifts and accurate photometry spanning the 4000Å break to the rest-frame *I*-band. Furthermore, emission-line luminosities are essential to accurately measure the current SFR (e.g., Brinchmann et al. 2004). The AEGIS Survey contains galaxies observed in a large wavelength range from X-ray to radio. From this catalog, we extract 6246 galaxies which have photometry at *B*, *R*, *I* (Coil et al. 2004) and K_s (Bundy et al. 2006). The resulting sample is magnitude-limited at K_s=22.5. From this sample, we select 4517 potentially star-forming galaxies ($U - B < 1.0$) that do not show contamination by an Active Galactic Nucleus (AGN). In particular, we reject the sources that are detected by *Chandra* and that are identified as AGNs following the criteria by Kauffmann et al. 2003 (rest-frame optical emission-line ratios), Yan et al. 2011 (rest-frame optical emission-line ratio versus color), and Donley et al. 2007 (slope of the *Spitzer* IRAC SED). For all 4517 galaxies, Keck/DEIMOS spectra are available from the DEEP2 Redshift Survey (Newman et al. 2012). They cover the wavelength range 6500-9100Å at a resolution of 1.4Å full width at half-maximum (FWHM). The accuracy of the redshifts is 30 km s^{-1}. Such resolution allows us also to extract reliable emission-line fluxes of [O II]$\lambda\lambda$3726.0,3728.8, Hβ, [O III]λ5007, and Hα when they fall into the observed wavelength range (Table 1). This set of photometric and spectroscopic data covers rest-frame wavelength ranges from $\lambda \sim$ 3300Å-1.8μm at $z = 0.2$ to $\lambda \sim$ 1650-9150Å at $z = 1.4$.

3. MODELING APPROACH

We derive precise constraints on the SFHs and stellar masses of galaxies using a sophisticated tool based on physically motivated models of SFH, stellar population synthesis, nebular emission and attenuation by dust. In this Section, we describe our library of models and how we fit the data.

3.1. *Library of model spectral energy distributions*

We build a comprehensive library of model star formation and chemical enrichment histories by performing a semi-analytic post-treatment of the Millennium cosmological simulation (Springel et al. 2005) using the models of De Lucia & Blaizot 2007. Following Pacifici et al. 2012, we use a sample of 100,000 galaxy SFHs from $z = 127$ to the present time. We then enlarge the model library by drawing 10 different realizations of the redshift of observation ($0.1 < z < 1.5$) and of the evolutionary stage for each galaxy (see Sections 2.1 and 3.1.2 in Pacifici et al. 2012) to account for the fact that galaxies can be observed at different stages of evolution. For each realization, we also resample the *current* (i.e., averaged over a period of 10 Myr before a galaxy is observed) specific SFR and gas-phase oxygen abundance, in the ranges $-2 < \log(\psi_S/Gyr^{-1}) < 1$ and $7 < 12 + \log(\mathrm{O/H}) < 9.4$, respectively, to avoid biases in parameter retrieval.

From this library of one million model SFHs, we generate SEDs by computing the emission from stars and gas. Details of how this is done are in Pacifici et al. 2012. The models rely on the latest version of the Bruzual & Charlot 2003 stellar population synthesis models and compute the nebular emission using the photoionization code CLOUDY as in Charlot & Longhetti 2001. We include the attenuation by dust with a two-component model as in Charlot & Fall 2000. For the dust model, we randomly choose the total optical depth of the dust ($\hat{\tau}_V$) between 0 and 3. Also for the dust model, we vary both the slope of the attenuation curve in the interstellar medium and the fraction of optical depth contributed by the dust in the interstellar medium in the ranges 0.4-1.1 and 0.1-0.7, respectively. Finally, to simulate the absorption by the intergalactic medium as a function of redshift, we adopt the prescription of Madau 1995.

This procedure allows us to go beyond the typical approach of using simple idealized functions at fixed metallicity to describe the SFHs of galaxies. However, one caveat is that our results may still depend on the star-formation prescriptions adopted in the semi-analytic model.

3.2. *Fitting procedure*

We use the final library of 1 million model galaxies described above to measure physical parameters for the 4517 galaxies with the multi-wavelength data presented in §2. We use a Bayesian approach, detailed in Pacifici et al. 2012. In brief, for each galaxy in our observational sample, we compute the likelihood that each model in the library describes the observations. Specifically, we fit to photometric fluxes in the observed *B*, *R*, *I* and K_s bands, in addition to emission-line luminosities of [O II], Hβ, [O III] and/or Hα. The exact lines fit depend on the rest-frame wavelength coverage of the spectra, as given in Table 1. Since galaxies in our observational sample have accurate spectroscopic redshifts, we compute likelihoods only for the model galaxies built within 0.05 of the spectroscopic redshift. We are thus fitting each observed galaxy with $\sim$ 71,500 models. For each galaxy, we use the computed likelihoods to build probability density functions (likelihood distributions) for the stellar mass and the SFR normalized to the absolute observed K_s-band luminosity. The typical uncertainties (defined as half of the 16th-84th percentile range of the cumulative probability density function) on the stellar masses and the SFRs are $\sim$ 0.1 and 0.3 dex, respectively. For each galaxy in the sample, we also derive the best-fit SFH.

4. STAR FORMATION HISTORIES OF BLUE GALAXIES

Blue galaxies form a distinct sequence in the parameter space of stellar mass and SFR (see e.g., Brinchmann et al. 2004, Noeske et al. 2007, Daddi et al. 2007, Whitaker et al. 2012), the SFR increasing systematically with mass and redshift. This is referred to as the "star-formation main sequence" (Noeske et al. 2007). In this Section, we examine the average SFHs of low- and high-mass galaxies as a function of redshift.

In Figure 1, we examine the best-fit SFH models for two example galaxies at similar redshifts, and which have similar *current* SFRs (ψ) but different stellar masses ($M_\star$). The first galaxy has a low stellar mass of $M_\star = 4.3 \times 10^9 M_\odot$ and $\psi = 4.8 M_\odot \mathrm{yr}^{-1}$. The second galaxy is more massive with $M_\star = 2.9 \times 10^{10} M_\odot$ and $\psi = 5.5 M_\odot \mathrm{yr}^{-1}$. It is interesting to note that the best-fit SFHs evolve inside the main sequence for their entire lifetimes. In the inset panels in Figure 1, the best-fit SFHs of these two galaxies are shown. These two SFHs show clearly the characteristic fluctuations over time that derive from the merging histories of the dark matter haloes and from the semi-analytic prescriptions used to model the baryonic component (gas infall, cooling, star formation, feedback). Neither of them would be well described

TABLE 1
MEDIAN STELLAR MASSES AND SFRS OF AEGIS GALAXIES

Redshift	Observed emission lines	$\log(M_*/M_\odot)$		$\log[\psi/(M_\odot \mathrm{yr}^{-1})]$		number of galaxies	
		low-mass[a]	high-mass[b]	low-mass[a]	high-mass[b]	low-mass[a]	high-mass[b]
$0.20 < z < 0.45$	Hβ, [O III], Hα	9.37	10.48	-0.185	0.375	167	16
$0.45 < z < 0.70$	Hβ, [O III]	9.40	10.56	-0.065	0.765	272	68
$0.70 < z < 0.85$	[O II], Hβ, [O III]	9.41	10.54	0.115	0.855	261	124
$0.85 < z < 1.10$	[O II], Hβ	9.43	10.52	0.625	1.155	191	105
$1.10 < z < 1.40$	[O II]	9.50	10.54	0.965	1.335	96	121

[a] Galaxies between 1.6 and $4.0 \times 10^9 M_*/M_\odot$ (blue dots in Figure 2)
[b] Galaxies between 2.5 and $6.3 \times 10^{10} M_*/M_\odot$ (green dots in Figure 2)

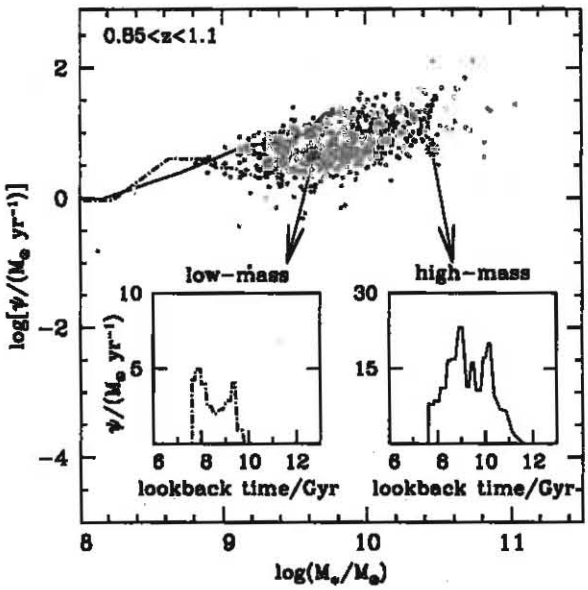

FIG. 1.— Measured SFR versus stellar mass for galaxies in the redshift range $0.85 < z < 1.1$ are shown as small grey points. The blue dash-dotted line shows the best-fit model SFH of an example low-mass galaxy, while the green solid line shows the best-fit model SFH of an example high-mass galaxy. Inserted panels show the SFR versus lookback time for these two example galaxies. Both best-fit models have significant variations with time and neither would be well described by a τ-model.

by a τ-model.

In Figure 2, we assess the shape of the average SFH of galaxies as a function of stellar mass and redshift. In the column on the left, we plot the star-formation main sequence for five redshift bins spanning 0.2-1.4. We explore two stellar mass bins which are sampled at all redshifts: a low-mass bin (1.6-4.0 $\times 10^9 M_*/M_\odot$) and a high-mass bin (2.5-6.3 $\times 10^{10} M_*/M_\odot$). Median stellar masses and SFRs in these two bins are given in Table 1. In the middle and right-hand columns, we plot the average best-fit SFHs of the galaxies in the low- and the high-mass bins, respectively, and the root mean squares about these averages. To compute the average SFH, we place the best-fit model SFH of each galaxy at the redshift of observation. We then co-add the individual SFHs as a function of cosmic time and divide by the number of galaxies that form stars at that time. The small deviations in the SFHs of individual galaxies (as shown by the example galaxies in Figure 1) are generally washed out by taking an average of many SFHs. However, they are still visible in the top right panel (high stellar mass, low redshift) since there are only 16 galaxies in this bin. The number of galaxies in each individual plot is listed in Table 1.

From Figure 2 is clear that the average SFH of low-mass galaxies is characterized by a *rising* function at all redshifts with a progressively steeper slope with increasing redshift. This is likely because high-redshift galaxies have had less time to form stars than galaxies at lower redshift. We find that high-mass galaxies on average form more quickly than low-mass galaxies. They are characterized by *bell-shaped* SFHs in which the SFR reaches a maximum and then declines. This is the case at all redshifts examined. From Figure 2 it is also clear that the lookback time at which galaxies have formed half of their total stellar mass shifts towards progressively higher lookback times with both increasing redshift of observation and increasing stellar mass. For high-mass galaxies it coincides with the peak of their SFR.

We make sure to include in our library a large variety of SFH *shapes*. These include shapes which are similar to declining, rising, bell-shaped and bursty. One way we have tested the robustness of our fits consists in examining the second and the third best-fit models for each galaxy. Doing so, the results shown in here do not change significantly.

5. DISCUSSION AND CONCLUSIONS

Popular cosmological scenarios predict that galaxies form hierarchically from the merger of many progenitors, each with their own unique SFH. With the maturity of semi-analytic models of galaxy evolution, we now have the ability to model the hierarchical build-up of galaxies. Therefore, we no longer need to rely on simple analytic descriptions of galaxy SFHs, and can adopt a more sophisticated approach.

In this work, we measure the SFHs of 4517 blue galaxies in the AEGIS Survey using a sophisticated library of model galaxy SEDs. We build this library by performing a semi-analytic post-treatment of the Millennium Simulation (Springel et al. 2005) and including the latest stellar population models along with prescriptions for nebular emission and attenuation by dust. For each galaxy, we retrieve the best-fit model SFH and the probability density functions of its stellar mass and SFR. We reach the following conclusions:

- The average SFH of high-mass galaxies rises and falls in a *bell-shaped* manner. This is inconsistent with simple exponentially-declining or rising τ-models.

- Low-mass galaxies have rising and extended SFHs, also inconsistent with τ-models. This implies that low-mass galaxies are currently more actively star-forming than high-mass galaxies. This is consistent with the trend in

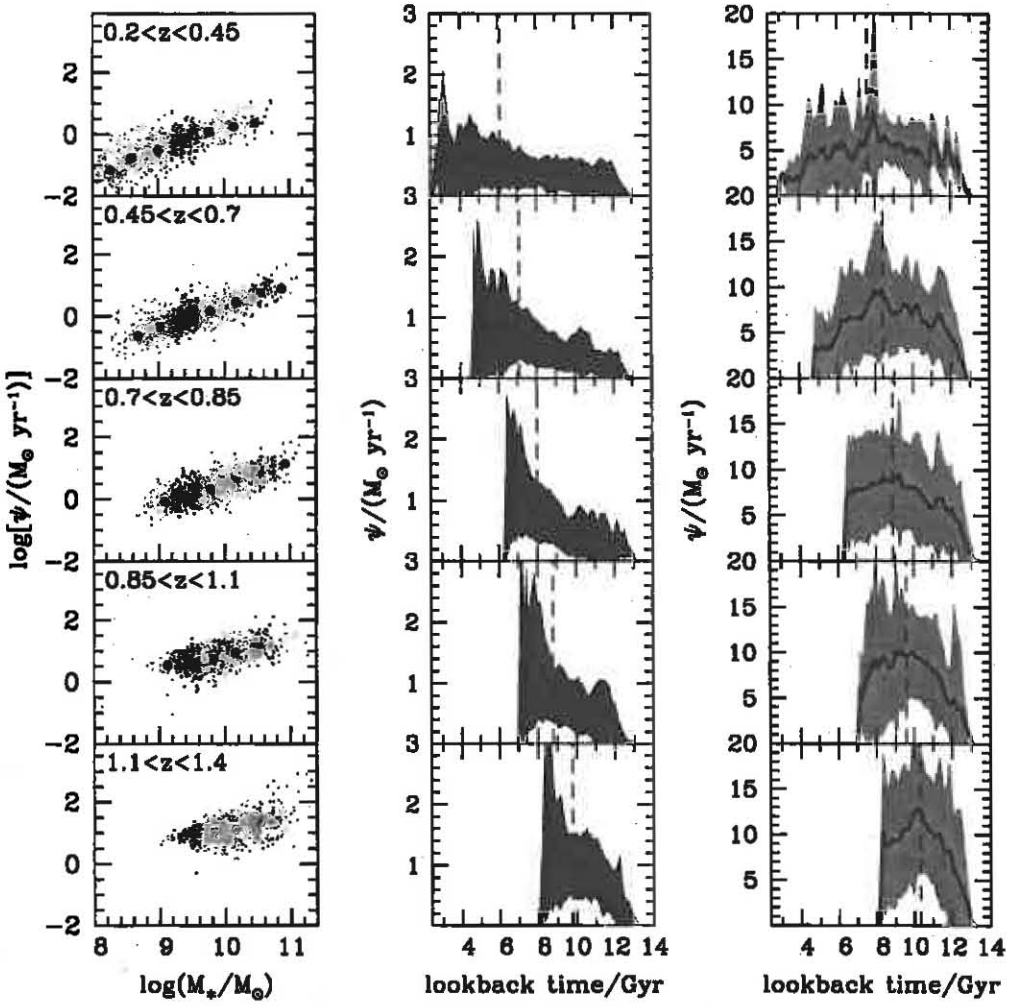

FIG. 2.— Left-hand column: Star-formation main sequence (i.e., SFR versus stellar mass) for the observed galaxies divided into five redshift bins spanning 0.2-1.4. Low-mass galaxies ($M_* = 1.6\text{-}4.0 \times 10^9 M_\odot$) are highlighted in blue, while high-mass galaxies ($M_* = 2.5\text{-}6.3 \times 10^{10} M_\odot$) are highlighted in green. Middle column: Average best-fit SFH of the low-mass galaxies (black solid line) and root mean square about this average (blue shadow). Right-hand column: Average best-fit SFH of the high-mass galaxies (black solid line) and root mean square about this average (green shadow). The average SFHs of high-mass galaxies rise and fall in a *bell-shaped* manner. Low-mass galaxies have rising and extended SFHs, and are therefore currently more actively star-forming than high-mass galaxies. Both low- and high-mass galaxy average SFHs are inconsistent with simple idealized τ-models.

the star-formation main sequence (Noeske et al. 2007) and with the latest simulations by Behroozi et al. 2012.

- The slopes of the average SFHs of both low- and high-mass galaxies are steeper at high redshift. This is likely because at high redshift, galaxies have less time to form stars compared with low redshift.

- On average, the time at which half the stellar mass in a galaxy has formed (vertical black dashed lines in Figure 2) is a function of both redshift of observation and stellar mass. It shifts towards progressively higher lookback times with increasing redshift of observation and increasing stellar mass. This is the case for both low- and high-mass galaxies.

- Both low- and high-mass galaxies evolve inside the star-formation main sequence for their entire lifetimes.

Our conclusions rely on physically motivated models of SFHs that can be used to interpret any type of observations. The work presented in this letter will be extended by using absorption lines in the spectra and observer-frame infrared photometry to improve the constraints on the SFHs (Pacifici et al. in preparation).

This work was funded in part by the Marie Curie Initial Training Network ELIXIR of the European Commission under contract PITN-GA-2008-214227. C.P. thanks the JWST Project and the Astrophysics Science Division at Goddard Space Flight Center for hosting her while working on this paper. S.A.K is supported by an appointment to the NASA Postdoctoral Program at NASA's Goddard Space Flight Center, administered by Oak Ridge Associated Universities through a contract with NASA. The authors also acknowledge NSF grants AST 95-29098 and 00-71198 to UC Santa Cruz. This study makes use of data from AEGIS, a survey conducted

with the Chandra, GALEX, Hubble, Keck, CFHT, MMT, Subaru, Palomar, Spitzer, VLA, and other telescopes and supported in part by the NSF, NASA, and the STFC.

REFERENCES

Behroozi, P. S., Wechsler, R. H., & Conroy, C. 2012, arXiv:1207.6105
Bell, E. F., & de Jong, R. S. 2001, ApJ, 550, 212
Brinchmann, J., Charlot, S., White, S. D. M., et al. 2004, MNRAS, 351, 1151
Bruzual, G., & Charlot, S. 2003, MNRAS, 344, 1000
Bundy, K., Ellis, R. S., Conselice, C. J., et al. 2006, ApJ, 651, 120
Chabrier, G. 2003, PASP, 115, 763
Charlot, S., & Fall, S. M. 2000, ApJ, 539, 718
Charlot, S., & Longhetti, M. 2001, MNRAS, 323, 889
Coil, A. L., Newman, J. A., Kaiser, N., et al. 2004, ApJ, 617, 765
Daddi, E., Dickinson, M., Morrison, G., et al. 2007, ApJ, 670, 156
Davis, M., Guhathakurta, P., Konidaris, N. P., et al. 2007, ApJ, 660, L1
De Lucia, G., & Blaizot, J. 2007, MNRAS, 375, 2
Donley, J. L., Rieke, G. H., Pérez-González, P. G., et al. 2007, ApJ, 660, 167
Kauffmann, G., Heckman, T. M., Tremonti, C., et al. 2003, MNRAS, 346, 1055
Klypin, A. A., Trujillo-Gomez, S., & Primack, J. 2011, ApJ, 740, 102
Lee, S.-K., Idzi, R., Ferguson, H. C., et al. 2009, ApJS, 184, 100
Madau, P. 1995, ApJ, 441, 18
Maraston, C., Pforr, J., Renzini, A., et al. 2010, MNRAS, 407, 830
Newman, J. A., Cooper, M. C., Davis, M., et al. 2012, arXiv:1203.3192
Noeske, K. G., Weiner, B. J., Faber, S. M., et al. 2007, ApJ, 660, L43
Pacifici, C., Charlot, S., Blaizot, J., & Brinchmann, J. 2012, MNRAS, 421, 2002
Papovich, C., Dickinson, M., & Ferguson, H. C. 2001, ApJ, 559, 620
Pforr, J., Maraston, C., & Tonini, C. 2012, MNRAS, 422, 3285
Reddy, N. A., & Pettini, M., & Steidel, C. C., et al. 2012, ApJ, 754, 25
Shapley, A. E., & Steidel, C. C., & Erb, D. K., et al. 2005, ApJ, 626, 698
Springel, V., & White, S. D. M., & Jenkins, A., et al. 2005, Nature, 435, 629
Stark, D. P., Ellis, R. S., Bunker, A., et al. 2009, ApJ, 697, 1493
Whitaker, K. E., van Dokkum, P. G., Brammer, G., & Franx, M. 2012, ApJ, 754, L29
Wuyts, S., Franx, M., Cox, T. J., et al. 2009, ApJ, 696, 348
Yan, R., Ho, L. C., Newman, J. A., et al. 2011, ApJ, 728, 38